

Energy & Environmental Science

Accepted Manuscript



This is an *Accepted Manuscript*, which has been through the Royal Society of Chemistry peer review process and has been accepted for publication.

Accepted Manuscripts are published online shortly after acceptance, before technical editing, formatting and proof reading. Using this free service, authors can make their results available to the community, in citable form, before we publish the edited article. We will replace this *Accepted Manuscript* with the edited and formatted *Advance Article* as soon as it is available.

You can find more information about *Accepted Manuscripts* in the [Information for Authors](#).

Please note that technical editing may introduce minor changes to the text and/or graphics, which may alter content. The journal's standard [Terms & Conditions](#) and the [Ethical guidelines](#) still apply. In no event shall the Royal Society of Chemistry be held responsible for any errors or omissions in this *Accepted Manuscript* or any consequences arising from the use of any information it contains.

Cite this: DOI: 10.1039/c0xx00000x

www.rsc.org/xxxxxx

ARTICLE TYPE

Surface termination and subsurface restructuring of Perovskite-based Solid Oxide Electrode Materials[†]

J. Druce^{a,*,+}, H. Téllez^{b,‡,*,+}, M. Burriel^{b,§}, M. D. Sharp^b, L. J. Fawcett^b, S. N. Cook^{b,1}, D. S. McPhail^b, T. Ishihara^a, H. H. Brongersma^c, and J. A. Kilner^{a,b,*}

⁵ Received (in XXX, XXX) Xth XXXXXXXXX 20XX, Accepted Xth XXXXXXXXX 20XX

DOI: 10.1039/b000000x

We study the outer atomic surfaces of a series of perovskite-based ceramics using Low Energy Ion Scattering spectroscopy. After high temperature treatment, segregated A-site (or acceptor substituent) cations dominate the outer surfaces with no B-site cations detected. We also find evidence of an associated B-cation enriched region below the surface.

Perovskite-based oxides are of growing importance because of their application in a diverse range of devices in clean energy, communications and microelectronics. The functional properties utilised range from ionic conductivity, magnetism, colossal magnetoresistance, superconductivity, dielectric and electrochemical properties, and examples of applications include solid oxide fuel cell electrodes, catalysts, gas sensors microwave dielectrics, and permanent magnets.[1] There is also intense current interest in the interface between thin film oxide structures due to reports of enhanced electronic and ionic conductivity.[2, 3] These structures are fabricated at elevated temperatures using either physical or chemical deposition techniques and clearly the immediate surface of the materials (and substrates) that form these layers can be of great importance in determining the functional properties of the resulting interfaces.

For all the above examples, the exchange of oxygen, at elevated temperatures, between the solid and the ambient gas, mediated by the immediate surface, is a very important process as it determines the oxygen stoichiometry and hence the functional properties. This gas-solid exchange will occur during any high-temperature processing step, such as deposition, sintering or annealing, and this interaction is fundamental to those materials used in high temperature electrochemical applications, such as electrodes for solid oxide fuel cells (SOFCs) and electrolyzers (SOECs). Clearly the surface composition of these materials has an important impact on the oxygen exchange kinetics, but it is only recently that interest is being directed towards the chemical characterization of the immediate surface and subsurface regions and its evolution under processing and operating conditions.

Most reported studies on oxide electroceramic surfaces use X-ray Photoelectron Spectroscopy (XPS)[4-6] and Secondary Ion Mass Spectrometry (SIMS)[7, 8]. Although both techniques are extremely useful to investigate the composition in the near surface region, information about the very outer surface is difficult to deconvolute as both integrate over several atomic layers (typically 2-3 for SIMS and 3-20 for XPS). This limitation

is absent for Low-Energy Ion Scattering (LEIS), which analyses only the very outer atomic monolayer, *i.e.* the very surface involved in reactions with the gas phase.[9] In LEIS, noble gas primary ions (typically He⁺, Ne⁺ or Ar⁺) are backscattered by elastic collisions with surface atoms of a sample, and their resulting kinetic energy distribution is analyzed. The kinematics of the backscattering event may be described as a two-body elastic collision, and the energy distribution of the backscattered ions is determined by the masses (and therefore elemental / isotopic identities) of the atoms in the outer surface of the sample.[9, 10] As well as providing compositional information specific to the very first atomic layer, the energy spectrum data is directly quantifiable due to the lack of matrix effects (unlike SIMS).[11] LEIS is therefore an ideal tool to probe the very outer layers of oxide electroceramics which determine their interaction with the surrounding gas phase.

In this work, we apply high sensitivity LEIS depth profiling to characterize the surface and near-surface composition of polycrystalline ceramics representative of the most promising perovskite-based mixed ionic and electronic conducting materials for fuel cell applications: La_{0.6}Sr_{0.4}Co_{0.2}Fe_{0.8}O_{3-δ} (LSCF-113, single perovskite), GdBaCo₂O_{5+δ} (GBCO-1125, double perovskite) and La₂NiO_{4+δ} (LNO-214, Ruddlesden-Popper *n*=1 structure).[12, 13]. The parent single perovskite ("113", from the A:B:O atomic ratios) crystal structure (ABO_{3-δ}) may be thought of as a stack of alternating AO and BO₂ sheets (Fig. 1a). These materials are often modified by adding aliovalent cations onto the A site (A'). If acceptor (A') and host (A) cations order in alternate AO planes, the double perovskite structure AA'B₂O_{5+δ} ("1125") shown in Fig. 1b is formed, with the AO –BO₂ – A'O –BO₂ stacking sequence. The final major family of interest is the Ruddlesden-Popper (RP) series of materials with a stacking sequence such as AO – (BO₂ – AO)_{*n*} –, and in particular the *n*=1 member of the family which corresponds to the A₂BO_{4+δ} structure ("214"). This may also be viewed as a series of *n* ABO₃ perovskite blocks, interspersed with AO rock salt planes. Note that for *n* equal to infinity, the structure would correspond to that of the parent perovskite phase.

After grinding and polishing to produce a flat, fresh surface, the samples were subjected to high temperature annealing treatments in order to simulate the processing and / or operation conditions (*i.e.* 1000°C for 12h in 200 mbar O₂) for their application in solid state electrochemical devices (see section in

Cite this: DOI: 10.1039/c0xx00000x

www.rsc.org/xxxxxx

ARTICLE TYPE

ESI[†] for further details on sample preparation). Since the surfaces were annealed for a significant amount of time at these elevated

temperatures, we expect them to be representative of the surfaces of the materials in practical devices.

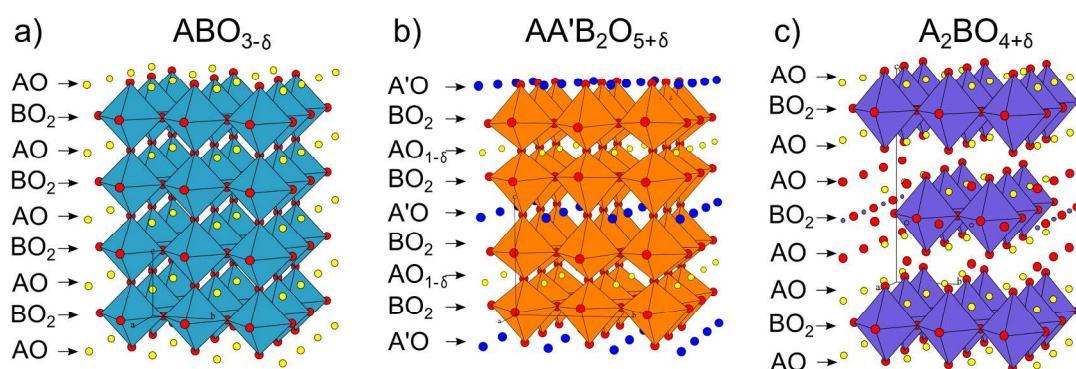


Fig.1 Structures of the perovskite and perovskite-related oxides studied in this work. (a) Perovskite structure ($ABO_{3-\delta}$), where A is the rare earth cation and B is the transition metal, (b) Ordered double perovskite ($AA'B_2O_{5+\delta}$), where A and A' cations are alternated in the layered structure, and (c) Ruddlesden-Popper structure with $n=1$ ($A_2BO_{4+\delta}$), where the perovskite unit cell is separated by the (AO) rock salt layers.

Prior to the LEIS analyses, the sample surfaces were exposed to atomic oxygen (at room temperature) in a sample preparation chamber attached to the instrument, in order to remove any hydrocarbon contaminants from exposure to the atmosphere. The absence of C was confirmed by analysis using 3 keV $^4\text{He}^+$ (Fig. S2 in ESI[†]). Once this cleaning was complete, a fresh area of the sample surface was selected for the depth profiling measurement. The depth profiles were acquired using a $^{20}\text{Ne}^+$ analysis beam and a 500 eV $^{40}\text{Ar}^+$ sputter beam incident at 59°. The Ne beam gives better separation for heavier masses, allowing us to resolve the peaks for the cations of interest during the depth profiling analyses. In order to ensure the information originated only from the very outer surface of the samples, the primary ion fluence used to acquire each spectrum was limited to ensure the analysis remained in the so-called “static regime”. Further details on the LEIS experiments are included in the ESI[†].

The immediate surfaces of all of the materials after a typical high temperature treatment in an oxidising ambient (Fig. 2, top plots) are dominated by one of the A-site cations. In the case of LNO-214, the lanthanum cation dominates the surface, whilst the LSCF-113 and GBCO-1125 materials partially substituted with divalent alkaline-earth cations also show an A-cation dominated surface, with strong preferential segregation of the substituent cations (A': Sr and Ba respectively). Whilst the surface of LNO-214 (Fig. 2c, top plot) does consist mainly of La, we also observe a very small peak (marked as *), which we assign to Pb. The Pb²⁺ acceptor substituent is known to segregate in perovskite ($(\text{La,Pb})\text{MnO}_3$, [14] leading to significant surface coverage in that case. Although the Pb content in the present LNO-214 starting powder is estimated to be less than 0.0015 wt. %, [15] impurity cations here could also segregate from the bulk to the outer surface of the pellet during the high temperature anneal (1000 °C, 12 h), causing the relatively low (a few tenths to a few percent) coverage we see here. Cross-contamination by volatile Pb species

from the annealing equipment cannot be excluded, although Pb contamination is not seen for the other samples studied here.

We detect no signal for the respective transition metal cations (B: Fe, Co and Ni) in the very outer surfaces of the polycrystalline samples. With light sputtering (sub-surface and “bulk” plots in Fig. 2), these peaks do appear clearly for layers just beneath the surface. The experimentally observed surface terminations are in striking contrast to the assumptions made in many computational modelling studies of the surface structure and oxygen exchange reaction, which assume either a mixed (AO)- and (BO₂)- terminated or a (BO₂)- dominated surface to facilitate electron transfer to reduce gaseous O₂. [16-22]

It is worth bearing in mind during the interpretation of the present data the polycrystalline ceramic nature of the samples. For example, the grain size of the single perovskite sample was around 2 μm; therefore, an analysis over an area of 1000 x 1000 μm² will probe the surfaces of around 250,000 grains, with a range of grain orientations. Although the polycrystalline ceramic samples contain many randomly orientated grains, the equilibrium surfaces will most likely show facets favouring only a few close packed, low index planes such as {100}, {110}, or {111}. Fullarton *et al.*, [23] compared the A:O coverage ratios for the acceptor-substituted perovskite $\text{Sm}_{1-x}\text{SrCoO}_3$ using external standards for surface atomic densities, and found surface coverages consistent with the (100) termination. Recent *ab initio* calculations by Ding *et al.*, [24] concur with this experimental observation, showing that (001) oriented slabs of $\text{La}_{0.5}\text{Sr}_{0.5}\text{FeO}_{3-\delta}$ were more stable than the (110) and (111) orientations.

The observed A-cation enriched surface layer is consistent with previous experimental reports for other single perovskite (isostructural to LSCF-113) materials, [4, 8, 23, 25-30] and LNO-214-based RP phases. [29, 31]. Additionally, many authors have shown evidence for the surface enrichment of acceptor substituents in perovskites including Sr²⁺ segregation in Sm_1 .

$x\text{Sr}_x\text{CoO}_{3-\delta}$, [23] $\text{La}_{1-x}\text{Sr}_x\text{MnO}_{3-\delta}$, [4, 32, 33] and $\text{La}_{0.6}\text{Sr}_{0.4}\text{Co}_{1-y}\text{Fe}_y\text{O}_{3-\delta}$, [26, 29, 34] as well as Pb^{2+} segregation in $(\text{La},\text{Pb})\text{MnO}_3$. [14]. Our results show the same trend for Ba^{2+} in the double perovskite GBCO-1125 (i.e. the A-site cation preferentially

located at the surface, with segregation of the A' acceptor substituent), suggesting that this termination is energetically favourable for all lanthanide-based perovskite-structured materials.

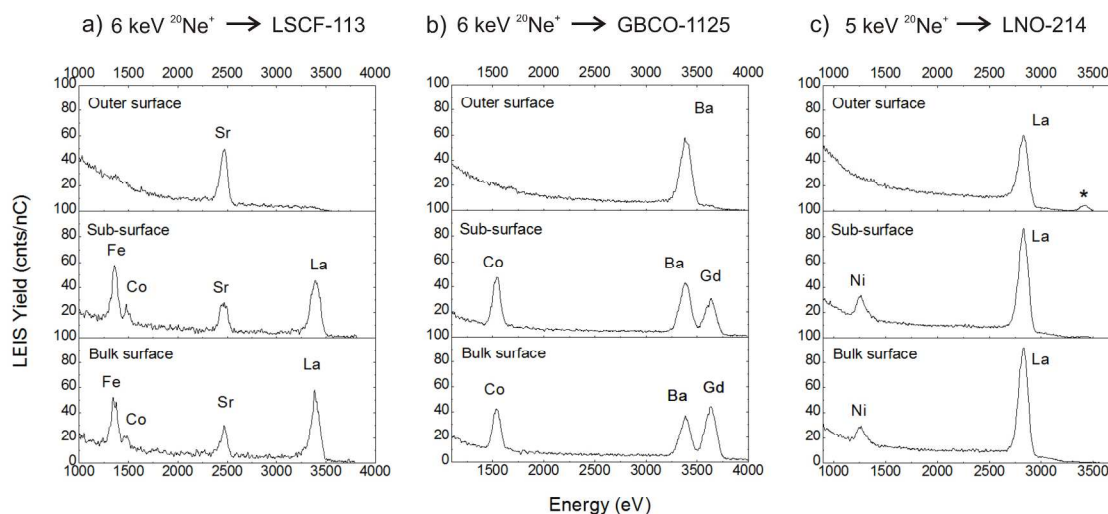


Fig. 2 LEIS spectra of the (a) single perovskite (LSCF-113), (b) double perovskite (GBCO-1125) and (c) Ruddlesden-Popper (LNO-214) samples after being annealed at 1000 °C for 12 hours at $p\text{O}_2 = 200$ mbar. Spectra are shown for the immediate outer surface (top row), sub surface after removal of a small amount of material by sputtering (middle row), and finally once the bulk composition has been reached (bottom row).

Whilst studies using techniques such as XPS, [4, 28, 30] SIMS [7, 8] or Total Reflection X-Ray Fluorescence (TXRF) [27] show enrichment of these cations towards the surface, we emphasise that the extreme surface sensitivity of our LEIS data (and previously reported studies on similar materials using this technique [23, 25, 26, 29, 31]) shows directly that the very outer atomic surfaces are totally dominated by the A-cations, with no detectable exposed transition metal cations.

Sputter depth profiles were then obtained using low energy Ar sputtering (500 eV, 59° incidence) to remove material, and the same $^{20}\text{Ne}^+$ analysis beam. These profiles, along with a description of the procedures used to calibrate them are given in the ESI[†] (Fig. S3[†]). In all samples, the profiles reveal three distinct regions, characterized by different cation ratios, as seen in fig. 3. Firstly, the very outermost surface is enriched in the A cation (particularly the acceptor substituent, A', if present). Light sputtering reveals the B cations, which grow in intensity to show a second region which is slightly enriched in these species compared to the bulk stoichiometry (dashed line in Fig. 3). Finally, after sufficient sputtering, the bulk composition is reached, showing a plateau in the cation surface coverage, which spectra corresponding to this bulk stoichiometric region are shown in the bottom row of Fig. 2). Analysis artefacts such as ion beam mixing and preferential sputtering that may be induced by the use of a sputtering-based technique have been carefully considered and can be neglected for these analyses, as justified in the ESI[†] (e.g. sputtering yields in Table S1[†]).

The profiles in fig. 3 allow us to quantify the extent of the surface segregation. In the acceptor doped materials (LSCF-113 and GBCO-1125) the aliovalent substituents (Sr^{2+} and Ba^{2+} respectively, denoted A') segregate strongly to the outermost surface. In both cases the A' site fraction is close to unity; in LSCF-113, the acceptor substituent site fraction ($A' / (A+A')$) is

0.97 at the surface, compared to 0.4 in the bulk (Fig. 3a), whilst GBCO-1125 shows a surface acceptor substituent fraction of 0.96, compared to 0.5 in the bulk.

The sputter depth profiles also reveal a distribution of the acceptor substituent with depth, which may be described by the expression $F_{(x)}^{A'} = b + \lambda e^{-x/G}$, similar to that used by Dulli *et al.* [4] to describe strontium segregation in $\text{La}_{0.65}\text{Sr}_{0.35}\text{MnO}_{3-\delta}$. In this equation, $F_{(x)}^{A'}$ represents the acceptor substituent site fraction at depth x , b is the bulk site fraction of the acceptor substituent (0.4 for LSCF-113 and 0.5 for GBCO-1125). The fitting parameters λ and G characterize the level of surface enrichment and the depth of the segregation profile respectively. However, whilst it was necessary to assume such a form in order to extract depth-resolved information from angle-resolved XPS data in ref. [4], we do not need to invoke such assumptions and see directly from our quantified LEIS data that the decay takes such a form.

Fitting the observed data to this equation yields values of $\lambda = 0.56$ and $G = 2.4$ nm for the single perovskite LSCF-113 and $\lambda = 0.50$ and $G = 2.97$ nm for the double perovskite GBCO-1125. Atomic mixing by the sputter beam could also produce an exponential decay in the LEIS signal, characterized by a mixing length similar to the mean projected range (R_p) of the sputtering beam. For the 500 eV $^{40}\text{Ar}^+$ sputter ions at 59 degrees incidence used here, R_p is estimated to be 1.0 nm for both the single and double perovskite. [35] Since this is less than half the value of the fitted G parameters, which characterize the segregation length, we discount the influence of ion beam mixing on the measured segregation profiles. In other words, these represent the “true” cation segregation profiles.

This segregation of the alkaline earth acceptor substituent (strontium in LSCF-113 and barium in GBCO-1125, respectively) is also consistent with literature reports for single perovskite materials, [4, 8, 14, 23, 26, 27, 32, 33, 36-38] and is thought to be driven by a combination of electrostatic and elastic

interactions caused by the size and charge mismatch of the substitutional ion.[24, 30] As shown in Fig. 1, the present materials consist of AO and BO₂ planes in different stacking sequences for the different perovskite related structures. A perovskite in which the A and B cations both have a charge of 3+ will therefore have planes of A³⁺O²⁻ and B³⁺O₂²⁻, which have overall positive and negative formal charges respectively. As discussed by Tasker,[39] cleaving such a crystal parallel to one of these charged planes (i.e. the (100) termination suggested above) will create an unstable polar surface with infinite associated

surface energy. In comparison, for the more commonly studied A²⁺B⁴⁺O₂²⁻ perovskites (e.g. SrTiO₃) both A²⁺O²⁻ and B⁴⁺O₂²⁻ planes will be formally neutral, and so the size mismatch between the host and substitutional cation will have more effect on the surface segregation behaviour. However, for perovskites in which the A and B cations have a charge of 3+, which are more typically used in electrochemical applications such as SOFC cathodes, the existence of surface charge will dominate the segregation behaviour.

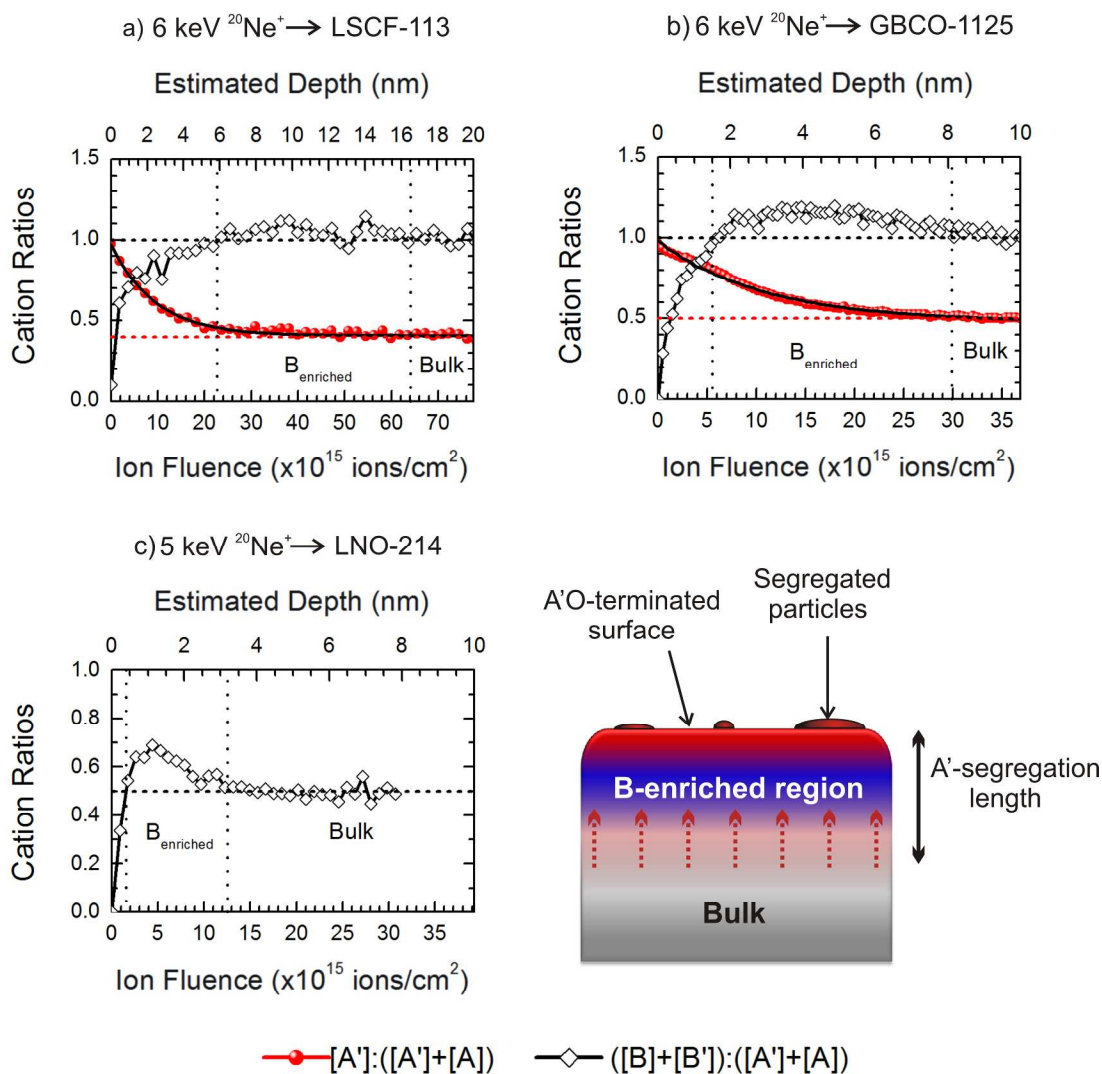


Fig. 3 LEIS depth profiles showing the acceptor substituent site fraction A':(A'+A) and the (B+B'):(A'+A) ratios at the surface and near-surface, for (a) LSCF-113, (b) GBCO-1125 and (c) LNO-214. Solid lines plotted for LSCF-113 and GBCO-1125 correspond to fittings to the expression from reference [4] to describe the divalent cation segregation, as explained in the text. (d) Schematic of compositional variations in near surface region of these perovskite electroceramics

Although replacing A³⁺ ions in the outer surface with A²⁺ ions will decrease the surface energy by neutralising the charged surface, Harrison[19] showed that a redistribution of the A-site cations with the A' substitutional exponentially enriched in the near surface region (i.e. as shown in the present data, as well as previous reports[4, 14]) is a lower energy solution to cancel the dipole moment near the surface and minimise surface energy.

However, Harrison's treatment predicts the lowest energy configuration to have segregation depths, G, of 0.31 and 0.21 nm

for the single and double perovskite respectively, clearly much lower than those measured for the polycrystalline samples here. Indeed the value Harrison predicts is also much lower than that measured experimentally for epitaxial films of La_{0.65}Sr_{0.35}MnO_{3-δ}. [4]

Whilst both surface charge and elastic interactions drive the surface segregation of acceptor substituents in ABO₃ perovskites,[24, 30] Harrison's theoretical description of the segregation profile neglects any strain effects, which may partly

account for the predicted segregation length being lower than observed experimentally. The second possible reason for the discrepancy, as acknowledged by Harrison, is that the theoretical treatment neglects the formation of any secondary phases at the material surface. Such phase changes may be in the form of oxide (AO), [40-43] hydroxide (AOH) [6, 44] or carbonate (ACO₃) [6] secondary phases at the sample surface, as is well known for A²⁺B⁴⁺O₃ perovskites such as SrTiO₃, and more recently reported in LSC. [44] Alternatively, structural rearrangement of the near surface of the perovskite into Ruddlesden-Popper type phases may occur. [4, 7, 45, 46] Since both phases are structurally related, this sub-surface reconstruction may also proceed in the opposite direction for the LNO-214 Ruddlesden-Popper phase, reconstructing into a higher order (e.g. $n = 2$ or 3) Ruddlesden-Popper phase, as previously described for LNO-214 single crystals. [47] Both of these mechanisms would be consistent with the (B+B' / A+A') profiles presented in Fig. 3 show evidence of a region a few nanometers below the surface which is enriched in the B cation (or depleted in the A cation) by a considerable factor of around 10%-20% for the LSCF-113 and GBCO-225 materials, and even higher (40%) for LNO-214, before the bulk stoichiometry is reached.

This sub-surface restructuring seems to be driven by the segregation of the A cations, or acceptor dopant (A') in A-site substituted perovskites, to the surface, although this does seem more sensitive to sample preparation and treatment conditions. Similar near-surface reconstruction has been suggested from XPS studies of La_{0.65}Sr_{0.35}MnO_{3-δ} thin films, where it was suggested that there may be some restructuring of the near-surface of the material into Ruddlesden-Popper type A_{n+1}B_nO_{3n+1} phases ($n = 1$ or 2) [4], as well as from SIMS analyses of A¹⁺B⁵⁺O₃ (KTaO₃) [46] and A²⁺B⁴⁺O₃ (SrTiO₃) [7] and BaTiO₃ [48]) perovskites, and attributed variously to A-cation deficient regions remaining after segregation of the A cation to the surface or as regions of B cation rich B_mO_{2m-1} Magneli phases. The correct interpretation of the SIMS profiles on which their conclusions were based is likely to be complicated somewhat by the challenges in quantifying such data, due to the matrix effects for which SIMS is notorious. However, this surface and sub-surface reconstruction seems to be a general trend in perovskite and related oxides as proved by the present LEIS depth profiles, which is free of the matrix effects and directly quantifiable even in the surface and near-surface regions.

In the case of LNO-214 the diffusion of La (A-site cation) towards the surface could result in a difference in the stacking sequence in the near-surface region which would lead to the appearance of Ruddlesden-Popper (RP) phases with $n > 1$ with a larger number of perovskite layers between each rock-salt layer. The appearance of both La₃Ni₂O_{7-δ} and La₄Ni₃O_{10-δ} $n = 2$ and $n = 3$ phases has been observed by Gauquelin *et al.* [47] for single crystal LNO-214 single crystals annealed in air at 1000 °C. The formation of the nickel-rich RP phases is believed to be due to near-surface segregation of nickel or evaporation of a volatile lanthanum species. [47, 49]

This A cation deficient region may not have been observed in the previous XPS measurements partly because its information depth (approximately 10 nm) is deeper than the that of LEIS. Furthermore, the interpretation of the angle resolved XPS data

relies on comparison of experimental data against elemental ratios calculated for an assumed model of the sample structure; if such an A-site cation deficiency is not incorporated into the model, then it may not be noticed in the data. This highlights one of the benefits of the LEIS depth profiling method used here; there is no need to invoke a model of the sample in order to extract quantitative information from the data.

Before concluding, we draw attention to fig. 3(d), which presents a schematic representation of the near-surface compositional variations in these perovskite-based materials suggested by our results. The very outer surface is dominated by the A-cation, or acceptor substituent. This is probably both still incorporated in the perovskite phase and precipitated as secondary phases. This segregation leaves a region which is depleted in the A-cation (or enriched in the B-cation), before the bulk stoichiometry is reached. If an acceptor substituent is present, an additional segregation profile of that substituent is superimposed on this, decaying exponentially from effectively unity at the surface to the bulk value.

Conclusions

The deviations in surface composition from bulk stoichiometry seen in these experiments using the new technique of high sensitivity LEIS are an illuminating insight into the dynamic nature of the outermost atomic layers of electroceramic materials. Significant surface modifications can occur after thermal treatments typical in processing and operation. These include temperatures and times similar to those used for calcining, sintering and the conditions used for thin film deposition. More importantly they correspond to the regimes used in the operational environments of high temperature devices such as solid oxide fuel cells. It is clear that significant reorganisation of an extended surface zone takes place. This surface zone is not simply a relaxation of the possible crystal termination, as is often modelled by DFT simulations, but a more extensive reorganisation of the atoms in this surface zone. What is also apparent is that the termination of those extremely important electroceramics with a (3,3) perovskite or perovskite related structure, show an overwhelming tendency to terminate in an AO plane and that when an alkaline earth is substituted for the trivalent A cation, this segregates very strongly to the outermost surface to remove any surface dipole moment.

A first question arises as to why this AO termination is the most stable at elevated temperatures (and high oxygen activities)? This predominant surface structure has profound implications for the catalytic activity of the materials as the transition metal cations, usually invoked as the active site for the interaction with any gaseous oxygen species, are hidden below the first atomic surface layer. As many of these materials do show high activity for catalytic processes such as oxygen reduction this implies that the presence of point defects, such as surface oxygen vacancies, which would expose the underlying transition metal cations, could have an extremely important role.

Acknowledgements

JD, JK and TI gratefully acknowledge the support of the International Institute for Carbon Neutral Energy Research (wpi-

¹²CNER), sponsored by the World Premier International Research Center Initiative (WPI), MEXT, Japan. HT and MB are funded by Marie Curie Intra European Fellowships within the 7th European Community Framework Programme of the European Union (PIEF-GA-2010-274999 and PIEF-GA-2009-252711, respectively). JD and HT contributed equally to this work.

Notes and references

⁺ These authors contributed equally to this work

^a International Institute for Carbon Neutral Energy Research (wpi-I2CNER), Kyushu University, Nishi-ku, Fukuoka, 819-0395, JAPAN. Email: john.druce@i2cner.kyushu-u.ac.jp; htellez@i2cner.kyushu-u.ac.jp; j.kilner@imperial.ac.uk. Tel: +81(0)92-802-6738 (JD,HT); +44(0)207-594-6745 (JK).

^b Department of Materials, Imperial College London, South Kensington, London, SW7 2AZ, UK.

^c Department of Applied Physics, Eindhoven University of Technology, P.O. Box 513, 5600 MB Eindhoven, The Netherlands.

[‡] Present affiliation: as (a)

[§] Present affiliation: Department of Advanced Materials for Energy, Catalonia Institute for Energy Research (IREC), Adria del Besòs, Barcelona, Spain

^{||} Present affiliation: Department of Materials Science and Engineering, Massachusetts Institute of Technology, Cambridge, MA 02139, USA

[†] Electronic Supplementary Information (ESI) available: Includes supplementary experimental details, figures and discussion. See DOI: 10.1039/b000000x/

1. Setter, N. and R. Waser, *Electroceraic materials*. Acta Materialia, 2000. **48**(1): p. 151-178.
2. Garcia-Barriocanal, J., et al., *Colossal Ionic Conductivity at Interfaces of Epitaxial ZrO₂:Y₂O₃/SrTiO₃ Heterostructures*. Science, 2008. **321**(5889): p. 676-680.
3. Ohtomo, A., et al., *Artificial charge-modulation in atomic-scale perovskite titanate superlattices*. Nature, 2002. **419**(6905): p. 378-380.
4. Dulli, H., et al., *Surface segregation and restructuring of colossal-magnetoresistant manganese perovskites La_{0.65}Sr_{0.35}MnO₃*. Physical Review B, 2000. **62**(22): p. R14629-R14632.
5. Crumlin, E.J., et al., *Surface strontium enrichment on highly active perovskites for oxygen electrocatalysis in solid oxide fuel cells*. Energy & Environmental Science, 2012. **5**(3): p. 6081-6088.
6. Jung, W. and H.L. Tuller, *Investigation of surface Sr segregation in model thin film solid oxide fuel cell perovskite electrodes*. Energy & Environmental Science, 2012. **5**(1): p. 5370-5378.
7. Szot, K., et al., *Restructuring of the surface region in SrTiO₃*. Applied Physics A, 1996. **64**(1): p. 55-59.
8. Kubicek, M., et al., *Relationship between Cation Segregation and Electrochemical Oxygen Reduction Kinetics of La_{0.5}Sr_{0.5}CoO_{3-d} Thin Film Electrodes*. J. Electrochem. Soc., 2011. **158**: p. B727.
9. Brongersma, H., et al., *Surface composition analysis by low-energy ion scattering*. Surface Science Reports, 2007. **62**(3): p. 63-109.
10. Brongersma, H.H., *Low-Energy Ion Scattering, in Characterization of Materials*, E.N. Kaufmann, Editor. 2012, John Wiley & Sons, Inc. New York. p. 2024-2044.
11. John Vickerman, I.G., *Surface Analysis: The Principal Techniques*. 2 ed. 2009: John Wiley & Sons.

12. Aguadero, A., et al., *Materials development for intermediate-temperature solid oxide electrochemical devices*. Journal of Materials Science, 2012. **47**(9): p. 3925-3948.
13. Tarancon, A., et al., *Advances in layered oxide cathodes for intermediate temperature solid oxide fuel cells*. Journal of Materials Chemistry, 2010. **20**(19): p. 3799-3813.
14. Borca, C.N., et al., *The surface phases of the La_{0.65}Pb_{0.35}MnO₃ manganese perovskite surface*. Surface Science, 2002. **512**(1-2): p. L346-L352.
15. CerPoTech, P.C.w., *Personal Communication*. 2013: London.
16. Read, M.S.D., et al., *Surface structures and defect properties of pure and doped LaNiO*. Journal of Materials Chemistry, 2001. **11**(10): p. 2597-2602.
17. Kotomin, E.A., et al., *Adsorption of atomic and molecular oxygen on the LaMnO₃(001) surface: ab initio supercell calculations and thermodynamics*. Physical Chemistry Chemical Physics, 2008. **10**(31): p. 4644-9.
18. Lee, Y.-L., et al., *Ab initio energetics of LaBO₃(001) (B=Mn, Fe, Co, and Ni) for solid oxide fuel cell cathodes*. Physical Review B, 2009. **80**(22).
19. Harrison, W.A., *Oxygen atoms and molecules at La_{1-x}Sr_xMnO₃ surfaces*. Physical Review B, 2010. **81**(4): p. 045433.
20. Mastrokov, Y.A., et al., *Pathways for Oxygen Incorporation in Mixed Conducting Perovskites: A DFT-Based Mechanistic Analysis for (La, Sr)MnO_{3-δ}*. The Journal of Physical Chemistry C, 2010. **114**(7): p. 3017-3027.
21. Han, J.W. and B. Yildiz, *Mechanism for enhanced oxygen reduction kinetics at the (La,Sr)CoO_{3-d}/(La,Sr)₂CoO_{4+d} hetero-interface*. Energy & Environmental Science, 2012. **5**(9): p. 8598-8607.
22. Zhou, J., et al., *Interaction of La₂NiO₄ (100) Surface with Oxygen Molecule: A First-Principles Study*. The Journal of Physical Chemistry C, 2013. **117**(25): p. 12991-12999.
23. Fullarton, I.C., et al., *Study of oxygen ion transport in acceptor doped samarium cobalt oxide*. Ionics, 1995. **1**: p. 51-58.
24. Ding, H., et al., *Suppression of Sr surface segregation in La_{1-x}Sr_xCo_{1-y}Fe_yO_{3-d}: a first principles study*. Physical Chemistry Chemical Physics, 2013. **15**(2): p. 489-96.
25. Rosink, J.J.W.M., J.P. Jacobs, and H.H. Brongersma, *The surface of the Perovskite powders LiBaF₃ and BaZrO₃ studied by low-energy ion scattering*. 1996. **378**: p. 44-51.
26. Viitanen, M.M., et al., *Silica poisoning of oxygen membranes*. Solid State Ionics, 2002. **150**(3-4): p. 223-228.
27. Fister, T.T., et al., *In situ characterization of strontium surface segregation in epitaxial La_{0.7}Sr_{0.3}MnO₃ thin films as a function of oxygen partial pressure*. Applied Physics Letters, 2008. **93**(15): p. 151904.
28. Cai, Z., et al., *Surface Electronic Structure Transitions at High Temperature on Perovskite Oxides: The Case of Strained La_{0.8}Sr_{0.2}CoO₃ Thin Films*. Journal of the American Chemical Society, 2011. **133**(44): p. 17696-17704.
29. Druce, J., T. Ishihara, and J. Kilner, *Surface composition of perovskite-type materials studied by Low Energy Ion Scattering (LEIS)*. Solid State Ionics, 2013(0).
30. Lee, W., et al., *Cation Size Mismatch and Charge Interactions Drive Dopant Segregation at the Surfaces of Manganite Perovskites*. Journal of the American Chemical Society, 2013. **135**(21): p. 7909-7925.
31. Burriel, M., et al., *Absence of Ni on the outer surface of Sr doped La₂NiO₄ single crystals*. Energy & Environmental Science, 2014. **7**(1): p. 311-316.
32. Ponce, S., M.A. Peña, and J.L.G. Fierro, *Surface properties and catalytic performance in methane combustion of Sr-substituted lanthanum manganites*. Applied Catalysis B: Environmental, 2000. **24**(3-4): p. 193-205.
33. Bertacco, R., et al., *Evidence for strontium segregation in La_{0.7}Sr_{0.3}MnO₃ thin films grown by pulsed laser deposition: consequences for tunnelling junctions*. Surface Science, 2002. **511**(1-3): p. 366-372.
34. Y. Teraoka, N.Y., T. Seiyama, *Surface States and Catalytic Properties of La_{1-x}Sr_xCoO₃*. Journal of the Surface Science Society of Japan, 1988. **9**: p. 153-158.

35. J.F. Ziegler, J.P.B., U. Littmark, *The Stopping and Range of Ions in Solids*. Vol. 1. 1985, New York, US: Pergamon.
36. Choi, J.W., et al., *Surfaces of the perovskite manganites $La_{1-x}Ca_xMnO_3$* . Physical Review B, 1999. **59**(20): p. 13453-13459.
37. Jiang, S.P. and J.G. Love, *Origin of the initial polarization behavior of Sr-doped $LaMnO_3$ for O_2 reduction in solid oxide fuel cells*. Solid State Ionics, 2001. **138**(3–4): p. 183-190.
38. Herger, R., et al., *Structure determination of monolayer-by-monolayer grown $La_{1-x}Sr_xMnO_3$ thin films and the onset of magnetoresistance*. Physical Review B, 2008. **77**(8): p. 085401.
39. Tasker, P.W., *The stability of ionic crystal surfaces*. Journal of Physics C: Solid State Physics, 1979. **12**(22): p. 4977.
40. Szot, K., et al., *Nature of the surface layer in ABO_3 -type perovskites at elevated temperatures*. Applied Physics A, 1996. **62**(4): p. 335-343.
41. Wei, H., et al., *Study of SrO segregation on $SrTiO_3(100)$ surfaces*. Journal of the European Ceramic Society, 2001. **21**(10–11): p. 1677-1680.
42. Gunhold, A., et al., *Geometric structure and chemical composition of $SrTiO_3$ surfaces heated under oxidizing and reducing conditions*. Surface Science, 2002. **507–510**(0): p. 447-452.
43. Chen, Y., et al., *Impact of Sr segregation on the electronic structure and oxygen reduction activity of $SrTi_{1-x}Fe_xO_3$ surfaces*. Energy & Environmental Science, 2012. **5**(7): p. 7979-7988.
44. Cai, Z., et al., *Chemical Heterogeneities on $La_{0.6}Sr_{0.4}CoO_{3-\delta}$ Thin Films—Correlations to Cathode Surface Activity and Stability*. Chemistry of Materials, 2012. **24**(6): p. 1116-1127.
45. Szot, K. and W. Speier, *Surfaces of reduced and oxidized $SrTiO_3$ from atomic force microscopy*. Physical Review B, 1999. **60**(8): p. 5909-5926.
46. Szot, K., et al., *Chemical inhomogeneity in the near-surface region of $KTaO_3$ evolving at elevated temperatures*. Journal of Physics: Condensed Matter, 2000. **12**(22): p. 4687.
47. Gauquelin, N., et al., *Long-term structural surface modifications of mixed conducting $La_2NiO_{4+\delta}$ at high temperatures*. Monatshefte für Chemie - Chemical Monthly, 2009. **140**(9): p. 1095-1102.
48. Szot, K., C. Freiburg, and M. Pawelczyk, *Layer structures BaO - $BaTiO_3$ in the region of p-type conductivity on the surface of $BaTiO_3$* . Applied Physics A, 1991. **53**(6): p. 563-567.
49. Egger, A., et al., *Long-Term Oxygen Exchange Kinetics of $Nd_2NiO_{4+\delta}$ in H_2O - and CO_2 -Containing Atmospheres*. Journal of The Electrochemical Society, 2010. **157**(11): p. B1537-B1541.

Surface termination and Subsurface Restructuring of Perovskite-based Solid Oxide Electrode Materials

Broader Context:

Perovskite-based (ABO_3) electro-ceramics have many applications including ferroelectrics, multiferroics and electro-catalysis in high temperature electrochemical devices. One subgroup, the $A^{3+}B^{3+}O_3$ (3,3 perovskites), are extensively used as electrode materials in solid oxide fuel cells and electrolyzers. These oxides contain a trivalent lanthanide cation on the A-site and a mixed valence transition metal cation on the B-site, with the lanthanide often partially substituted by a divalent alkaline earth to promote electrocatalysis. Their catalytic activity is often related to the nature of the B-site transition metal cation. Our results using a surface analysis technique sensitive to the very outermost atomic layer show, very unexpectedly, that the B-site transition metal cations are not exposed at the surface to participate in catalytic reactions, to within the detection limits of the technique. In fact, we show that for three representative perovskite-based electro-ceramics, the larger A-site cations dominate the surface leaving a transition metal rich region beneath the surface. Substitution by a divalent alkaline earth cation leads to a strong preferential segregation of this cation to the surface. These findings indicate the importance of characterizing the surfaces of these materials at the atomic level for the understanding of catalytic and oxygen exchange performance. Furthermore, they provide a basis to guide fundamental theoretical studies of the exchange of oxygen between the gas ambient and the electrochemically-active surfaces of perovskite-based ceramics.